In Situ Studies of the Active Sites for the Water Gas Shift Reaction over Cu−CeO_2 Catalysts: Complex Interaction between Metallic Copper and Oxygen Vacancies of Ceria

Xianqin Wang,[†] José A. Rodriguez,*[,†] Jonathan C. Hanson,[†] Daniel Gamarra,[‡] Arturo Martínez-Arias,*[,‡] and Marcos Fernández-García*[,‡]

Chemistry Department, Brookhaven National Laboratory, Upton, New York 11973, and Instituto de Catálisis y Petroleoquímica, CSIC, Campus Cantoblanco, 28049 Madrid, Spain

Received: September 26, 2005; In Final Form: October 27, 2005

New information about the active sites for the water gas shift (WGS) reaction over Cu−CeO_2 systems was obtained using in-situ, time-resolved X-ray diffraction (TR-XRD), X-ray absorption spectroscopy (TR-XAS, Cu K and Ce L_3 edges), and infrared spectroscopy (DRIFTS). Cu−CeO_2 nanoparticles prepared by a novel reversed microemulsion method (doped $Ce_{1-x}Cu_xO_2$ sample) and an impregnation method (impregnated CuO_x/CeO_2 sample) were studied. The results from all of the samples indicate that both metallic copper and oxygen vacancies in ceria were involved in the generation of active sites for the WGS reaction. Evidence was found for a synergistic Cu−$O_{vacancy}$ interaction. This interaction enhances the chemical activity of Cu, and the presence of Cu facilitates the formation of O vacancies in ceria under reaction conditions. Water dissociation occurred on the $O_{vacancy}$ sites or the Cu−$O_{vacancy}$ interface. No significant amounts of formate were formed on the catalysts during the WGS reaction. The presence of strongly bound carbonates is an important factor for the deactivation of the catalysts at high temperatures. This work identifies for the first time the active sites for the WGS reaction on Cu−CeO_2 catalysts and illustrates the importance of in situ structural studies for heterogeneous catalytic reactions.

Introduction

Nowadays, we face new challenges in creating alternate fuels, cleaning the environment, dealing with the causes of global warming, and keeping us safe from toxic substances and infectious agents.[1] Hydrogen is a potential solution for satisfying many of our energy needs while reducing (and eventually eliminating) carbon dioxide and other greenhouse gas emissions.[2] At present, nearly 95% of the hydrogen supply is produced from the reforming of crude oil, coal, natural gas, wood, organic wastes, and biomass.[3] The reformed fuel contains 1−10% CO, which degrades the performance of the Pt electrode in fuel cell systems.[4] To get clean hydrogen for fuel cells and other industrial applications, the water gas shift (WGS) reaction ($CO + H_2O \rightarrow CO_2 + H_2$) and CO oxidation ($2CO + O_2 \rightarrow 2CO_2$) processes are critical.[3] To accelerate them, heterogeneous catalysts are frequently used.[5] A fundamental understanding of the configuration and properties of the active sites for the WGS reaction is a prerequisite for designing catalysts with a high activity or efficiency.[5]

In this work, the behavior of CuO_x/CeO_2 and $Ce_{1-x}Cu_xO_2$ catalysts for the WGS reaction is investigated. CeO_2-based catalysts have been reported to be very promising for the WGS reaction owing to the peculiar redox properties of ceria and its oxygen storage capacity.[5] CuO−CeO_2 mixed-metal oxides have important applications as electrodes in fuel cells[6] and gas sensors[7] and as efficient catalysts for various reactions, such as the combustion of CO and methane,[8−11] the WGS,[11−13] the reduction of SO_2 by CO,[14] methanol synthesis,[15] and the wet oxidation of phenol.[16] It is anticipated that with proper development, metal-promoted ceria catalysts should realize much higher CO conversions in the WGS than commercial Cu/ZnO catalysts.[13,17−19]

The roles played by the ceria and copper in the WGS over Cu−CeO_2 catalysts are a matter of debate.[16−22] Either metallic Cu or Cu^{1+} cations have been proposed as active sites for the WGS reaction.[22] Ceria may not be a simple spectator and may play a direct role in the catalytic process.[20,21] Concerning the reaction mechanism, there is no agreement, either. A mechanism with formate ($CO + OH \rightarrow HCOO$) as an intermediate formed on partially reduced ceria has been proposed[13] in which the breaking of the C−H bond in the formate was the rate-limiting step for the WGS. On the other hand, a redox reaction ($CO + O \rightarrow CO_2$) was alternatively proposed to be the rate-limiting step by other authors.[12] They also suggested that Cu was the active site for the catalysis and that ceria had no effect on the activity.[12] In a similar way, metallic copper was proposed to be the only active species for the steam reforming of dimethyl ether,[23] whereas the copper/ceria interface was reported to be the active phase for the steam reforming of methanol or CO oxidation reactions.[9,24]

In situ characterization of the Cu−CeO_2 catalysts under operational conditions is critical to clarify the roles of ceria and Cu. In recent works, time-resolved X-ray diffraction (TR-XRD) and time-resolved X-ray absorption fine structure (TR-XAFS) were employed to study in situ the interaction of copper oxides or ceria with H_2 and CO at atmospheric pressures.[25−28] These powerful techniques, the product of combining the high intensity of synchrotron radiation with rapid, new, parallel data-collection devices, allowed a systematic study of the kinetics and mechanism for the reduction of CuO, Cu_2O, and CeO_2.[26−29] In this article, in situ TR-XRD, TR-XAFS, and infrared spectroscopy (DRIFTS) are employed to examine the behavior of CuO_x/CeO_2

[†] Chemistry Department, Brookhaven National Laboratory.
[‡] Instituto de Catálisis y Petroleoquimica.

10.1021/jp055467g CCC: $33.50
Published on Web 12/08/2005

and $Ce_{1-x}Cu_xO_2$ nanoparticles under different WGS reaction conditions and gas environments.

Materials and Characterization Methods

Materials Preparation. The reference CuO, Cu_2O, and Cu bulk samples used in this work were obtained from Alfa-Aesar (>99.99% purity). Cu-doped ceria, labeled as $Ce_{1-x}Cu_xO_2$ ($x = 0.05$ or 0.2) was prepared with a modified reversed microemulsion method.[25,30] The precursors were introduced in a reverse microemulsion (water in oil) using *n*-heptane as the organic phase, Triton X-100 (Aldrich) as surfactant, and hexanol as cosurfactant. Then this suspension was mixed with another similar suspension containing an alkali solution (tetramethylammonium hydroxide, Aldrich) as aqueous phase. All cations were coprecipitated, and the resulting mixtures were stirred for 24 h, centrifuged, decanted, and rinsed with methanol. Finally, the solid portion was dried overnight at 100 °C, and the resulting powders were calcined under air at 500 °C for 2 h. Full details of the preparation parameters employed can be found elsewhere.[30] ICP-AES chemical analysis of these samples confirmed quantitative precipitation of both Cu and Ce cations. Surface area values (S_{BET}) obtained for these samples were observed to increase with the copper content (130 and 151 $m^2\ g^{-1}$ for $Ce_{0.95}Cu_{0.05}O_2$ and $Ce_{0.8}Cu_{0.2}O_2$, respectively), in correlation with the size decrease observed in the oxide nanoparticles.[31]

The sample of copper supported on CeO_2 (5% weight in Cu, denoted hereafter as 5Cu) was synthesized by incipient wetness impregnation of a CeO_2 support, prepared by microemulsion in a similar manner as described above, with a copper nitrate aqueous solution. Following impregnation, the sample was dried overnight at 100 °C and, finally, calcined under air at 500 °C for 2 h. The S_{BET} value obtained for this sample prepared by impregnation was 101 $m^2\ g^{-1}$, close to that of the parent CeO_2 support.

In Situ Time-Resolved X-ray Diffraction. In situ time-resolved X-ray diffraction (TR-XRD) experiments were carried out on beam line ×7B of the National Synchrotron Light Source (NSLS) at Brookhaven National Laboratory. The sample was loaded into a sapphire capillary cell that was attached to a flow system.[25−27]A small resistance heater was wrapped around the capillary, and the temperature was monitored with a 0.1-mm chromel−alumel thermocouple that was placed straight into the capillary near the sample. Two-dimensional powder patterns were collected with a Mar345 image plate detector, and the powder rings were integrated using the FIT2D code.[32] The instrument parameters (Thompson−Cox−Hastings profile coefficients and Berar−Baldinozzi asymmetry correction) were derived from the fit of a Si reference pattern. Lattice constants were determined by a Rietveld analysis using the GSAS (General Structure Analysis System) program.[33] Diffraction patterns were collected over the catalysts during the WGS reaction and in different gas environments including 5% CO/He, 5% H_2O/He, and 5% O_2/He (named as gas-switch experiment). The WGS reaction was carried out isothermally at several temperatures (200, 300, 400, and 500 °C) with a 5% CO and 95% He gas mixture at a flow rate of ∼10 mL/min [or a space velocity, defined as (volumetric feed flow rate)/(catalyst volume), of $\sim 1.5 \times 10^5$/h]. This gas mixture passed through a water tube before entering the reactor. The relative ratio of water vapor pressure to CO in the gas mixture was ∼0.6.

In Situ Time-Resolved X-ray Absorption. Cu K-edge and Ce L_3-edge XAFS spectra were collected in air at room temperature and in situ under different operation conditions, similar to those for the TR-XRD experiments, at beamline ×18B of the NSLS. The same cell was used for the XAFS experiments as that for in situ XRD, except that the sample was loaded into a Kapton capillary (DuPont) and heated with hot air. The X-ray absorption spectra were taken repeatedly in the "fluorescence yield mode" using a pips detector cooled with circulating water. XAFS data have been analyzed using the Athena and Artimis programs.[34] They allow background removal by optimization of the low-*R* portion of the EXAFS data (i.e., minimizing the average value of the low-*R* Fourier transform, maintaining at the same time the value for the first coordination shell at maximum).[35]

The products from both TR-XRD and TR-XAFS experiments were measured with a 0−100 amu quadrupole mass spectrometer (QMS, Stanford Research Systems). A portion of the exit gas flow passed through a leak valve and into the QMS vacuum chamber. QMS signals at mass-to-charge ratios of 2(H_2), 4(He), 12(C), 15(CH_3), 17(OH), 18(H_2O), 28(CO), 32(O_2), and 44(CO_2) were monitored during the experiments, and these were recorded at the same time by an online computer.

In Situ DRIFTS. In situ DRIFTS analysis of the samples under WGS reaction conditions was carried out using a Bruker Equinox 55 FTIR spectrometer fitted with an MCT detector. The DRIFTS cell (Harrick) was fitted with CaF_2 windows and a heating cartridge that allowed samples to be heated to 500 °C. Samples of ∼100 mg were exposed to 3% H_2O and 5% CO (He balance) at a flow corresponding to $1.5 \times 10^5\ h^{-1}$ space velocity. The catalysts were heated under the reactant flow using a ramp of 10 °C min^{-1}. The heating ramp was stopped every 100 °C for recording a spectrum (average of 50 scans at 4 cm^{-1} resolution) after achieving steady state conditions based on the product concentration measured simultaneously with a mass spectrometer.

Results and DIscussion

Chemical State of Cu During the WGS Reaction. *5% CuO_x/CeO_2 Sample.* A typical set of time-resolved X-ray diffraction patterns is shown in Figure 1a for the 5% CuO_x/CeO_2 (denoted as 5Cu) impregnated sample during the WGS reaction at different temperatures. A copper oxide phase was clearly observed at the beginning of experiments at 25 °C and transformed to metallic copper as soon as the temperature was increased to 300 °C. By comparing the product curves (Figure 1b) with the XRD patterns, it is clear that the signals for H_2 and CO increase concomitantly with the appearance of metallic copper, indicating the important role of this species during the water gas shift reaction. The concentration of products increased when the temperature was raised to 400 °C, but it decreased at 500 °C, pointing to a deactivation of the 5Cu sample at high temperature, probably due to the production of strongly bound carbonate species (see below) that poison the active sites of the catalyst.[22,36]

Similar experiments were carried out with in situ time-resolved XAFS. Figure 2a displays the Fourier transforms of the Cu K-edge EXAFS spectra collected over the 5Cu sample cooled to room temperature after the WGS reaction at 25, 200, 300, and 400 °C. The position of the main peak located between 1.1 and 2.0 Å at room temperature, which corresponds to the first Cu−O coordination shell, is similar to that of CuO.[26] The Cu−O peak decrease was combined with an increase in the Cu−Cu peak in metallic copper and disappeared at high temperatures. The product curves from in-situ XAFS experiments were not shown here, since they were similar to those for in-situ TR-XRD experiments. The results confirmed the important role of metallic copper in the WGS reaction also observed in in situ XRD results.

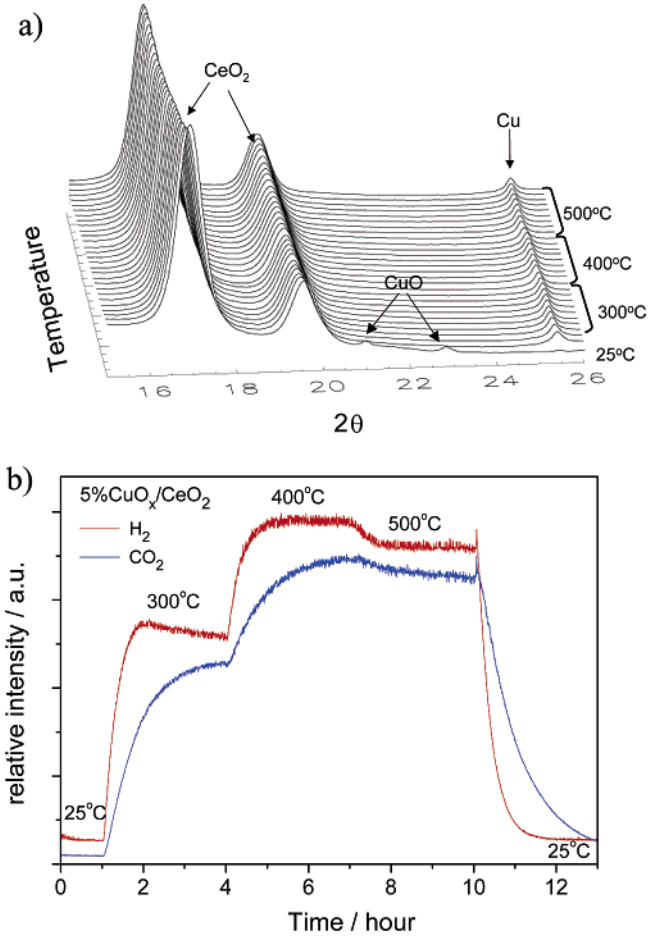

Figure 1. (a) Time-resolved X-ray diffraction patterns for 5% CuOx/CeO_2 catalyst during the water gas shift reaction at different temperatures (λ = 0.922 Å). (b) The relative concentration of H_2 and CO_2 products as a function of time at different temperatures during the water gas shift reaction as shown in (a).

Cu-Doped Ceria Samples. The WGS activity of the $Ce_{1-x}Cu_xO_2$ compounds was tested with a methodology similar to that described above for the 5% CuO_x/CeO_2 catalyst. Figures 2b and 3 show the results for the $Ce_{0.8}Cu_{0.2}O_2$ sample. The Cu K-edge EXAFS spectra were collected working at reaction temperatures of 25, 100, 200, 300, and 400 °C. Under WGS reaction conditions, Cu atoms in $Ce_{0.8}Cu_{0.2}O_2$ were seen to transform to Cu_2O at 100 °C (as was confirmed by the line shape of the FT trace and the peak at ~3.1 Å characteristic of Cu_2O),[31] then to metallic copper at elevated temperatures. However, WGS activity was detected with the mass spectrometer (data not shown) only after the formation of metallic copper. The corresponding XRD patterns in Figure 3 indicate that no copper or copper oxides were observed at low temperatures. It must be taken into account in this respect that under these conditions, the Cu atoms are more or less uniformly distributed through the bulk and the surface of the ceria particles.[31] However, clear features for metallic copper were seen at temperatures above 150 °C, and their intensity increased when raising the temperature. This reveals that copper sinters during reduction under WGS conditions in this sample, as shown to occur also under H_2 in a previous work.[31] The mass spectrometer signals for H_2 and CO_2 in Figure 3b show a low WGS activity at temperatures below 220 °C, and much higher activity at 300 and 400 °C with the presence of metallic copper. Very similar results were found when examining the behavior of a $Ce_{0.95}Cu_{0.05}O_2$ catalyst.

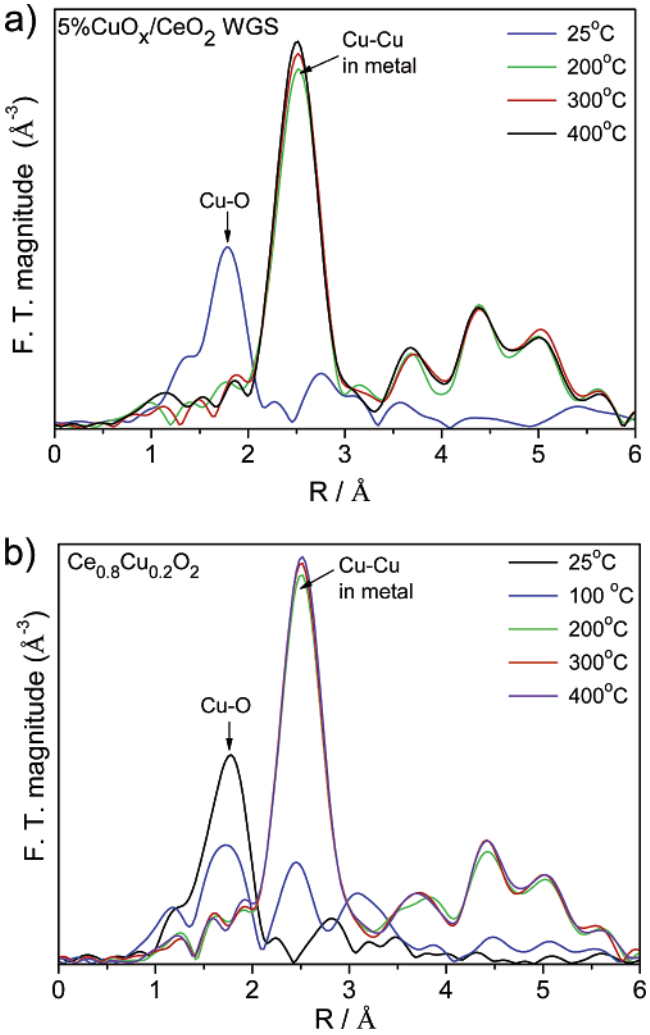

Figure 2. (a) Cu K-edge EXAFS spectra collected over 5% CuOx/CeO_2 cooled down to room temperature after the water gas shift reaction at different temperatures. (b) Cu K-edge EXAFS spectra collected over $Ce_{0.8}Cu_{0.2}O_2$ cooled down to room temperature after the water gas shift reaction at different temperatures.

In summary, the in-situ studies of TR-XRD and TR-XAFS show that metallic copper plays a vital role in the WGS reaction over both CuOx/CeO_2 and $Ce_{1-x}Cu_xO_2$ catalysts. The copper oxide species initially present in the catalysts must undergo a complete reduction before any substantial WGS activity is seen.

WGS Activity Comparison for Different Cu−CeO_2 Samples. Figure 4 compares the production of H_2 during the WGS reaction over the same amount (~5 mg) of CuO, $Ce_{0.8}Cu_{0.2}O_2$, $Ce_{0.95}Cu_{0.05}O_2$, and 5% CuO_x/CeO_2 at different temperatures. No activity was observed over pure nano ceria under the present operating conditions. Figure 4 clearly indicates that the impregnated 5% CuO_x/CeO_2 sample had better WGS activity than those of doped samples. The catalyst based on pure CuO had little activity. This catalyst certainly had the largest concentration of copper sites among the studied samples. These results indicate that interactions between copper and ceria enhance the activity of the metal in Cu−CeO_2 catalysts, suggesting that the WGS reaction may take place preferentially on the copper/ceria interface. In the next section, we will examine these options and the behavior of ceria during the WGS reaction.

Reduction/Oxidation of Ceria under Different Gas Environments. It is well-known that oxygen vacancies are easily formed in ceria nanoparticles.[25] In Cu−CeO_2 samples, there are

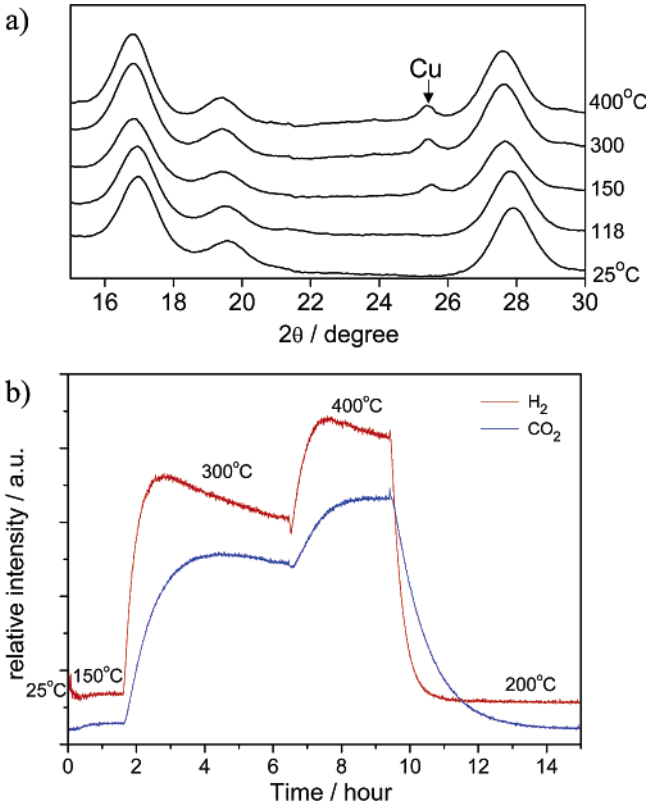

Figure 3. Time-resolved X-ray diffraction patterns for $Ce_{0.8}Cu_{0.2}O_2$ catalyst during the water gas shift reaction at different temperatures (λ = 0.992 Å). (b) The relative concentration of H_2 and CO_2 products as a function of time at different temperatures during the water gas shift reaction as shown in (a).

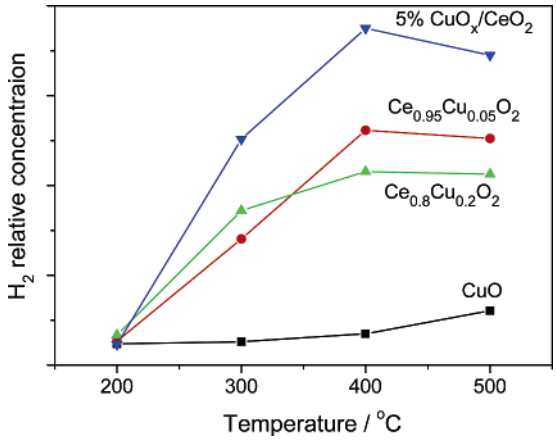

Figure 4. Relative concentrations of H_2 produced from the WGS reaction at different temperatures over 5% CuOx/CeO_2, $Ce_{0.8}Cu_{0.2}O_2$, $Ce_{0.95}Cu_{0.05}O_2$, and CuO using the same operating conditions (space velocity ~1.5 × 10^5/h).

two main processes to form oxygen vacancies: Ce^{4+} reduction and Cu^{2+} replacement in the ceria lattice.[31] In the reduction process, two Ce^{4+} cations are reduced to two Ce^{3+} cations with one oxygen vacancy formed ($2Ce^{4+} + O^{2-} \rightarrow 2Ce^{3+} + O_{vac}$). Since Ce^{3+} is bigger with respect to Ce^{4+}, a simple reduction leads to a ceria lattice cell expansion.[25] Different from the reduction process, the ceria lattice cell will slightly contract if one Cu^{2+} cation replaces one Ce^{4+} cation with one oxygen vacancy ($Ce^{4+} + O^{2-} \rightarrow Ce^{4+} + Cu^{2+} + O_{vac}$).[31] Thus, changes in the lattice parameter can be directly related to the concentration of oxygen vacancies and Cu atoms in ceria. Variations in the ceria lattice were studied exposing the 5% Cu/CeO_2 and $Cu_{0.2}Ce_{0.8}O_2$ samples to He, 5% CO/He, WGS reaction conditions (H_2O/CO ~ 0.6), H_2O/He, or 5% O_2/He at different temperatures. The changes in the chemical state of Ce during the WGS reaction were monitored by taking in situ Ce L_3-edge XANES spectra.

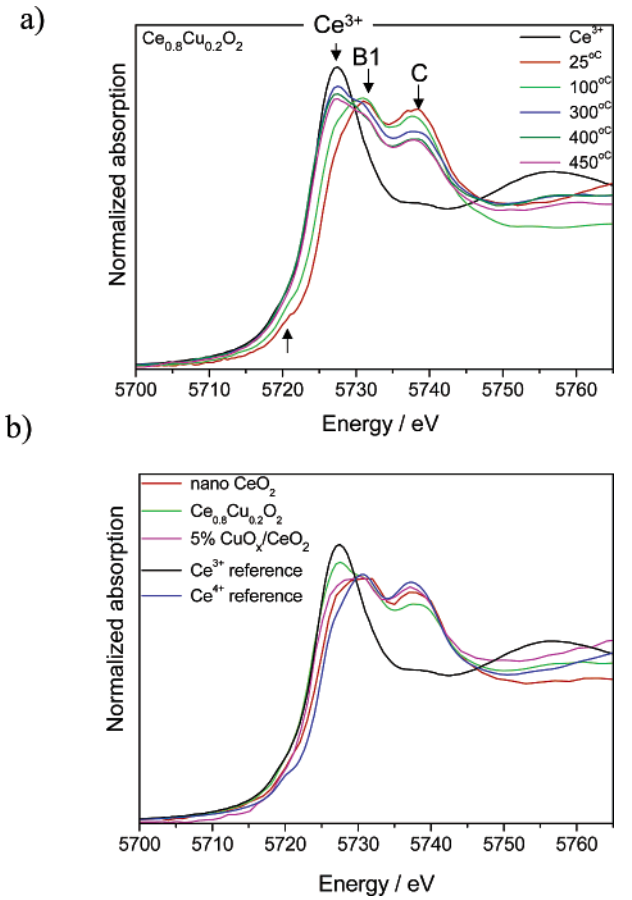

Figure 5. Ce L_3-edge XANES spectra collected over $Ce_{0.8}Cu_{0.2}O_2$ during the water gas shift reaction at different temperatures. (b) Ce L_3-edge XANES spectra collected over 5% CuOx/CeO_2, $Ce_{0.8}Cu_{0.2}O_2$, nano ceria during the WGS reaction at 300 °C, and references of bulk CeO_2 and $Ce(NO_3)_3 \cdot 6H_2O$.

Ce L_3-Edge TR-XANES Results. The Ce L_3 edge is frequently used as a "fingerprint" to characterize the electronic properties of ceria-based materials.[37] The electronic transitions behind these XANES features are complex. In pure stoichiometric CeO_2, the Ce L_3 edge exhibits two clear peaks, frequently labeled B_1 and C. A third peak, with lower photon energy than B_1, can be obtained by curve fitting.[37]

Figure 5a compares the Ce L_3-edge XANES spectra from the $Ce_{0.8}Cu_{0.2}O_2$ sample in the water gas shift reaction at different temperatures with the spectrum for a $Ce(NO_3)_3 \cdot 6H_2O$ reference, in which the cerium atoms are trivalent. The two main peaks in the spectrum of the sample at room temperature are separated by ~7 eV, in agreement with previous results.[25,26,37]. On the basis of the comparison of the intensities of the spectra near the Ce^{3+} position, we were able to confirm that oxygen vacancies and Ce^{3+} were formed during the WGS reaction. The amount of oxygen vacancies and Ce^{3+} were seen to increase with the increase in reaction temperature up to 300 °C, but decreased at higher temperatures, especially above 400 °C. When the $Ce_{0.8}Cu_{0.2}O_2$ catalyst was exposed to 5% CO in He, the amount of Ce^{3+} formed was bigger than for the experiments in Figure 5a and increased continuously with the temperature of exposure. These results show that ceria was oxidized by H_2O under the WGS reaction, with oxygen vacancies and Ce^{3+} being eliminated, especially at high temperature.

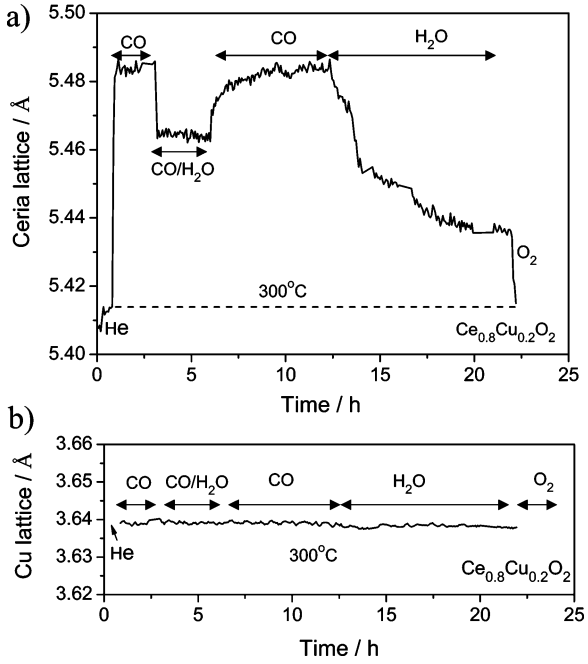

Figure 6. Lattice parameters during the gas-switch experiments over $Ce_{0.8}Cu_{0.2}O_2$ at 300 °C: (a) ceria and (b) metallic copper.

Figure 5b presents the Ce L_3-edge XANES spectra for $Ce_{0.8}Cu_{0.2}O_2$, 5% CuO_x/CeO_2 and nano ceria collected during the WGS reaction at 300 °C plus reference spectra for bulk ceria and $Ce(NO_3)_3 \cdot 6H_2O$ standards. The peak intensities at the Ce^{3+} position for the three samples followed the order $Ce_{0.8}Cu_{0.2}O_2$ > 5% CuO_x/CeO_2 > nano ceria, pointing out the improved ceria reducibility for the Cu-containing ceria samples, as reported in the literature.[9a,21a] In accordance with this, the closer interaction between copper and ceria in the mixed-metal oxide (or its higher copper dispersion, compare Figures 1a and 3a) certainly explains the higher ceria reducibility in it (Figure 5b).

Variations in Ceria Lattice during the WGS. Figure 6shows the lattice parameters for ceria (Figure 6a) and metallic Cu (Figure 6b) determined from (111) diffraction peaks of TR-XRD patterns for $Cu_{0.2}Ce_{0.8}O_2$ in different gases at 300 °C. The sample was first heated to 300 °C in He, and no metallic Cu was observed (Figure 6b). Metallic copper was formed as soon as the gas was switched to 5% CO/He, stayed through the WGS reaction and H_2O exposure, and disappeared after O_2 oxidation. The disappearance of metallic Cu and the practical recovery of the initial lattice parameter in an oxygen environment confirms that the reduction and oxidation of Cu and Ce in $Ce_{0.8}Cu_{0.2}O_2$ is reversible.[31] The lattice of the formed metallic Cu did not change under different gas environments of CO and H_2O. In contrast, the ceria lattice varied significantly (Figure 6a) with an increase after exposure to CO and a decrease in H_2O, indicating that CO reduced ceria, and H_2O oxidized it. In other words, CO created oxygen vacancies, and H_2O eliminated them. The water−ceria interaction is a complex process and is closely related to the surface termination and morphology of ceria.[38] In this work, the H_2O oxidation of CeO_{2-x} is consistent with studies over ceria powders[39,40] and films of CeO_2(111) grown on Ru (0001).[41] A comparison of the ceria lattices in Figure 6 for oxidation in water and O_2 indicates that H_2O does not completely reoxidize the CeO_{2-x}. The ceria lattice parameter under the WGS reaction reflects a combination of the effects of CO reduction and H_2O oxidation, implying that oxygen vacancies on the fluorite phase are involved in the chemistry of the process.

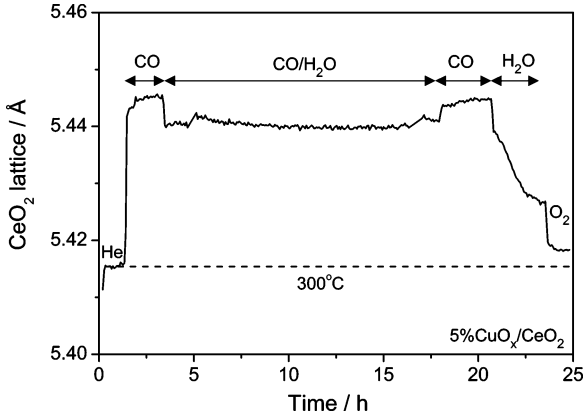

Figure 7. Ceria lattice parameters in the gas-switch experiments over 5% Cu/CeO_2 at 300 °C (a) ceria and (b) metallic copper.

The XRD/XAFS results described above show that both metallic copper and oxygen vacancies in ceria are involved in the active sites for the WGS reaction. It is clear that neither copper nor the O vacancies alone have the chemical properties necessary for the high WGS activity seen over the Cu−CeO_2 catalysts. From previous studies with single crystals and films, it is well known that metallic copper is more active than pure CuO_x for the WGS.[42] Recent studies performed in our laboratory have shown that the O vacancies in ceria are very efficient for the chemical activation of gold nanoparticles,[43] and the same probably occurs for copper nanoparticles.[44] Which one plays the leading role in the WGS, copper or the O vacancies? To answer this question, gas-switch experiments were also carried out over the 5% CuO_x/CeO_2 catalyst, and the ceria lattice parameters in different gas environments are presented in Figure 7. A comparison shows that the variations in the ceria lattice parameters for the $Ce_{0.8}Cu_{0.2}O_2$ sample (Figure 6a) were much larger than those for the 5% CuO_x/CeO_2 sample under WGS reaction conditions, CO/He or H_2O/He environments, indicating the presence of a higher concentration of oxygen vacancies and Ce^{3+} in the $Ce_{0.8}Cu_{0.2}O_2$ sample. However, as shown in Figure 4, the activity for the 5% CuO_x/CeO_2 sample was significantly higher than that for the $Ce_{0.8}Cu_{0.2}O_2$ sample. Thus, the activity of the Cu−CeO_2 catalysts did not correlate directly with the amount of oxygen vacancies or Ce^{3+} in the ceria support, pointing to the leading role of metallic Cu. The lower activity of the $Ce_{0.8}Cu_{0.2}O_2$ sample could be due to the smaller amount of surface metallic Cu atoms, since some Cu metal particles can remain embedded in the ceria lattice and could not be easily accessible to the reactants. On the other hand, carbonate species, which may become poisons of the WGS reaction,[22,36] could affect to a greater extent the $Ce_{0.8}Cu_{0.2}O_2$ catalyst, considering the higher copper dispersion in it and the fact that formation of such species is strongly promoted by the presence of copper−ceria interfaces in this type of catalyst.[45] This point will be investigated in more detail in the next section.

Generation of OH and CO_3 Groups on the Cu−CeO_2 Catalysts: In Situ FTIR Studies. To understand what causes the variations in activity seen in Figure 4, in situ DRIFTS experiments were carried out over the $Ce_{0.8}Cu_{0.2}O_2$ and 5% CuO_x/CeO_2 samples. The corresponding spectra are shown in Figure 8a and b, respectively; activity profiles obtained during these runs (not shown) were similar to those presented in Figure 4. The spectra from both samples indicated the formation of a Cu^+ carbonyl species (showing a characteristic band in the 2120−2100 cm^{-1} range)[9b] at relatively low reaction temperatures (displaying a maximum at 100 °C), in fair agreement with XAFS results (Figure 2). Significant amounts of carbonate (or

related) species (whose most intense bands appear in the 1800−1200 cm^{-1} range) were formed at a temperature as low as 100 °C, and their intensities increased with an elevation of the reaction temperature. Monodentate carbonates (bands at ∼1480 and 1390 cm^{-1})[46] and bidentate carbonates or carboxilates (bands or shoulders at ∼1550 and 1330 cm^{-1}) were formed at 100 °C, and a minor amount of formate species (bands or shoulders at ∼2935, 2845, 1590, and 1360 cm^{-1})[47] appeared at 300 °C and displayed stronger intensity for $Ce_{0.8}Cu_{0.2}O_2$. Other bands observed in the spectra are those corresponding to interacting hydroxyl species (broad band in the 3500−3000 cm^{-1} range), the intensities of which became stronger with increasing reaction temperature. Perusal of the spectra show a weak band overlapped on the R-branch of CO(g) (at ∼2175 cm^{-1}) for the spectra recorded at 300 °C that may correspond to an electronic transition, in particular, configurations of Ce^{3+}.[9b,48]

In general, two main reaction mechanisms have been proposed for the WGS over metal-promoted ceria catalysts.[12,13,20] In one of them, H_2O dissociates on the surface of the catalyst, forming OH groups that then react with CO to yield formate intermediates.[13] The formates react with water, producing H_2 and unidentate carbonates (rate-limiting step), which in the final step decompose to generate CO_2.[13a] This reaction mechanism is probably not dominating the chemistry on the Cu−CeO_2 catalysts, since the intensity of surface formate peaks seen in the DRIFT data of Figure 8 is very small or negligible, and furthermore, no correlation is found between this observable and the respective catalytic activities (Figures 4 and 8). In a second proposed reaction mechanism,[12,20] CO bonds to metal sites and then reacts with ceria to form CO_2 and O vacancies in the support. The water undergoes decomposition on the O vacancies to generate H_2.[20] The data in Figures 6, 7, and 8 are clear evidence of the feasibility of a redox-type reaction mechanism for the Cu−CeO_2 catalysts.

Comparing the data in Figures 4 and 8, the highest catalytic activity of 5% CuO_x/CeO_2 could be a consequence of a large concentration of copper on the surface that facilitates the dissociation of water (larger IR signal for OH groups). In addition, the $Ce_{0.8}Cu_{0.2}O_2$ exhibits a stronger signal for carbonates, and this could prevent the Ce^{3+}/Ce^{4+} redox interplay at the metal−promoter interface and poison active sites of the catalyst.[22,36] An indication that this type of phenomenon could be occurring in this catalyst at high temperature was obtained from the Ce L_3 results discussed above. Moreover, the possibility of ceria over-reduction has been discussed recently as being a factor that would increase carbonate stability, resulting in surface poisoning.[49] So a careful balance between the redox state of Cu and CeO_2 phases could be needed for optimum catalytic activity, and this may not only concern interface zones of both constituents but also suffer from a medium to large range influence. For 5% CuO_x/CeO_2, the catalytic activity decrease at temperatures above 400 °C can be related to the significant increase in the coverage of carbonates.

Conclusions

In situ DRIFTS, time-resolved X-ray diffraction, and (Cu K-edge and Ce L_3-edge) X-ray absorption spectroscopy were used to identify the active sites for the WGS reaction on CuO_x/CeO_2 and $Ce_{1-x}Cu_xO_2$ catalysts. The results from all the samples indicate that both metallic copper and oxygen vacancies in ceria are involved in the generation of the catalytically active sites. Evidence was found for a synergistic Cu−$O_{vacancy}$ interaction. This interaction enhances the chemical activity of Cu, and the presence of Cu facilitates the formation of O vacancies in ceria. H_2O dissociation occurred on the $O_{vacancy}$ sites or the Cu−$O_{vacancy}$ interface. In situ DRIFTS indicates that the amount of formate formed during the WGS reaction on the Cu−CeO_2 catalysts is very small or negligible and does not correlate with the activity results. The presence of strongly bound carbonates appears to be an important factor for explaining the catalytic properties of these systems, including deactivation at high temperatures. This work identified for the first time the active sites for the WGS reaction on Cu−CeO_2 catalysts and illustrates the importance of in situ structural studies for heterogeneous catalytic reactions.

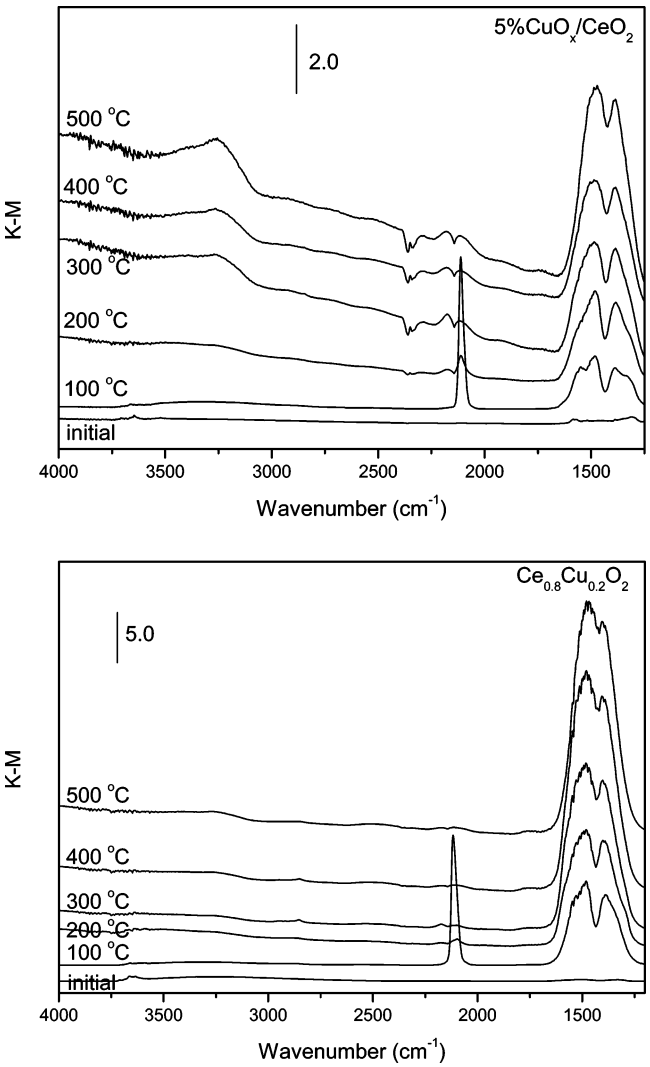

Figure 8. In situ DRIFTS spectra recorded under 3% H_2O and 5% CO at the indicated temperatures over 5% CuOx/CeO_2. (b) In situ DRIFTS spectra recorded under 3% H_2O and 5% CO at the indicated temperatures over $Ce_{0.8}Cu_{0.2}O_2$.

Acknowledgment. The research carried out at the Chemistry Department of Brookhaven National Laboratory was financed through Contract No. DE-AC02-98CH10086 with the U.S. Department of Energy, Division of Chemical Sciences. The NSLS is supported by the Divisions of Materials and Chemical Sciences of DOE. Work at the ''Instituto de Catálisis (CSIC)" was done with financial support from CICYT (Contracts No. CTQ2004-03409/BQU and MAT2003-03925). D. G. thanks the FPI program of the Ministerio de Educación y Ciencia for a PhD grant. Thanks are due to Syed Khalid and Wolfgang Caliebe for their help and facilities given in the operation of

beamlines ×18B and ×19A and Zhong Zhong for his help in the operation of beamline ×17B1 of the NSLS.

References and Notes

(1) Energy Policy Act (EPAct), 1992.

(2) (a) President's Hydrogen Initiative, 2003. (b) Jacobson, M. Z.; Colella, W. G.; Golden, D. M. *Science* **2005**, *308*, 1901.

(3) (a) Spivey, J. J. *Catal. Today* **2005**, *100* (1−2), 171. (b) Tonkovich, A. Y.; Zilka, J. L.; LaMont, M. J.; Wang, Y.; Wegeng, R. S. *Chem. Eng. Sci*. **1999**, *54*, 2947.

(4) (a) Liu, Y.; Fu, Q.; Flytzani-Stephanopoulos, M. *Catal. Today* **2004**, *93*−*95*, 241. (b) Suh, D. J.; Kwak, C.; Kim, J. H.; Kwon, S. M.; Park, T. J. *J. Power Sources* **2005**, *142* (1−2), 70.

(5) Li, Y.; Fu, Q.; Flytzani-Stephanopoulos, M. *Appl. Catal., B* **2000**, 27, 179.

(6) (a) Inoue, T.; Setoguchi, T.; Eguchi, K.; Arai, H. *Solid State Ionics* **1989**, *34*, 285. (b) Park, S.; Vohs; J. M.; Gorte, R. J. *Nature* **2000**, *404*, 265. (c) Gorte, R. J.; Vohs, J. M.; McIntosch, S. *Solid State Ionics* **2004**, *175*, 1.

(7) Lampe, U.; Gerblinger, J.; Meixner, H. *Sens. Actuators* **1992**, *B7*, 787.

(8) (a) Kau, L.-S.; Solomon, D. J.; Penner-Haln, J. E.; Hodgson, K. O.; Solomon, E. I. *J. Am. Chem. Soc.* **1987**, *109*, 6433. (b) Skårman, B.; Grandjean, D.; Benfield, R. E.; Hinz, A.; Andersson, A.; Wallenberg, L. R.; *J. Catal*. **2002**, *211*, 119, and references therein.

(9) (a) Martínez-Arias, A.; Hungría, A. B.; Fernández-García, M.; Conesa, J. C.; Munuera, G. *J. Phys. Chem. B* **2004**, *108*, 17983, and references therein. (b) Martínez-Arias, A.; Fernández-García, M.; Soria, J.; Conesa, J. C. *J. Catal.* **1999**, *182*, 367, and references therein. (c) Martínez-Arias, A.; Fernández-García, M.; Gálvez, O.; Coronado, J. M.; Anderson, J. A.; Conesa, J. C.; Soria, J.; Munuera, G. *J. Catal.* **2000**, *195*, 207.

(10) Harrison, P. G.; Ball, I. K.; Azelee, W.; Daniell, W.; Goldfarb, D. *Chem. Mater*. **2000**, *12*, 3715.

(11) (a) Liu, W.; Flytzani-Stephanopoulos, M. *J. Catal.* **1995**, *153*, 304. (b) Liu, W.; Flytzani-Stephanopoulos, M. *J. Catal.* **1995**, *153*, 317. (c) Qi. X.; Flytzani-Stephanopoulos, M. *Ind. Eng. Chem. Res*. **2004**, *43*, 3055. (d) Shan, W.; Shen, W.; Li, C. *Chem. Mater*. **2003**, *15*, 4761.

(12) (a) Bunluesin, T.; Gorte, R. J.; Graham, G. W. *Appl. Catal., B* **1998**, *15*, 107. (b) Koryabkina, N. A.; Phatak, A. A.; Ruettinger, W. F.; Farrauto, R. J.; Ribeiro, F. H. *J. Catal.* **2003**, *217*, 233.

(13) (a) Shido, T.; Iwasawa, Y. *J. Catal.* **1993**, 141, 71. (b) Jacobs, G.; Chenu, E.; Patterson, P. M.; Williams, L.; Sparks, D.; Thomas, G.; Davis, B. H. *Appl. Catal., A* **2004**, *258*, 203.

(14) Zhu, T.; Kundakovic, L.; Dreher, A.; Flytzani-Stephanopoulos, M. *Catal. Today* **1999**, *50*, 381.

(15) Shaw, E. A.; Rayment, T.; Walker, A. P.; Lambert, R. M.; Gauntlett, T.; Oldman, R. J.; Dent, A. *Catal. Today* **1991**, *9*, 197.

(16) (a) Hočevar, S.; Batista, J.; Levec, J. *J. Catal.* **1999**, *184*, 39. (b) Hočevar, S.; Krasovec, U.O.; Orel, B.; Arico, A. S.; Kim, H. *Appl. Catal., B* **2000**, *28*, 113.

(17) Liu, Y.; Hayakama, T.; Suzuki, K.; Hamakawa, S. *Catal. Commun.* **2001**, *2*, 195.

(18) Men, Y.; Gnaser, H.; Zapf, R.; Hessel, V.; Ziegler, C.; Kolb, G. *Appl. Catal., A* **2004**, *277*, 83.

(19) Papavasiliou, J.; Avgouropoulos, G.; Ioannides, T. *Catal. Commun*. **2004**, *5*, 231.

(20) (a) Bunluesin, T.; Gorte, R.; Graham, G. *Appl. Catal., B* **1998**, *15*, 107. (b) Hilaire, S.; Wang, X.; Luo, T.; Gorte, R. J.; Wagner, J. *Appl. Catal., B* **2001**, *215*, 271.

(21) (a) Li, Y.; Fu, Q.; Flytzani-Stephanopoulos, M. *Appl. Catal., B* **2000**, *27*, 179. (b) Fu, Q.; Weber, A.; Flytzani-Stephanopoulos, M. *Catal. Lett.* **2001**, *77* (1−3), 87.

(22) (a) Tschöpe, A.; Schaadt, D.; Birringer, R.; Ying, J. Y. *Nanostruct. Mater.* **1997**, *9*, 423. (b) Ovensen, C. V.; Stolze, P.; Nørskov, J. K.; Campbell, C. T. *J. Catal.* **1992**, *134*, 445.

(23) Matsumoto, T.; Nishiguchi, T.; Kanai, H.; Utani, K.; Matsumura, Y.; Imamura, S. *Appl. Catal., A* **2004**, *276*, 267.

(24) Men, Y.; Gnaser, H.; Zapf, R.; Hessel, V.; Ziegler, C.; Kolb, G. *Appl. Catal., A* **2004**, *277*, 83.

(25) (a) Wang, X. Q.; Hanson, J. C.; Liu, G.; Rodriguez, J. A.; Iglesias-Juez, A.; Fernández-García, M. *J. Chem. Phys*. **2004**, *121*, 5434. (b) Wang, X.; Hanson, J. C.; Rodriguez, J. A.; Belver, C.; Fernández-García, M. *J. Chem. Phys*. **2005**, *122*, 154711.

(26) Wang, X.; Hanson, J. C.; Frenkel, A. I.; Kim, J.-Y.; Rodriguez, J. A. *J. Phys. Chem. B* **2004**, *108*, 13667.

(27) Kim, J. Y.; Rodriguez, J. A.; Hanson, J. C.; Frenkel, A. I.; Lee, P. L. *J. Am. Chem. Soc*. **2003**, *125*, 10684.

(28) Rodriguez, J. A.; Hanson, J. C.; Kim, J.-Y.; Liu, G.; Iglesias-Juez, A.; Fernández-García, M. *J. Phys. Chem. B* **2003**, *107*, 3535.

(29) Rodriguez, J. A.; Wang, X. Q.; Liu, G.; Hanson, J. C.; Hrbek, H.; Peden, C. H. F.; Iglesias-Juez, A.; Fernández-García, M. *J. Mol. Catal. A: Chem.* **2005**, *228*, 11.

(30) (a) Fernández-García, M.; Martínez-Arias, A.; Guerrero-Ruiz, A.; Conesa, J. C.; Soria, J. *J. Catal*. **2002**, *211*, 326. (b) Iglesias-Juez, A.; Hungría, A. B.; Gálvez, O.; Martínez-Arias, A.; Fernández-García, M.; Conesa, J. C.; Soria, J. *Stud. Surf. Sci. Catal*. **2001**, *138*, 347. (c) Fernández-García, M.; Martínez-Arias, A.; Hungría, A. B.; Iglesias-Juez, A.; Conesa, J. C.; Soria, J. *Phys. Chem. Chem. Phys*. **2002**, *4*, 2473. (d) Hungria, A. B.; Martínez-Arias, A.; Fernández-García, M.; Iglesias-Juez, A.; Guerrero-Ruiz, A.; Calvino, J. J.; Conesa, J. C.; Soria, J. *Chem. Mater*. **2003**, *15*, 4309. (e) Martínez-Arias, A.; Fernández-García, M.; Ballesteros, V.; Salamanca, L. N.; Conesa, J. C.; Otero, C.; Soria, J. *Langmuir* **1999**, *15*, 4796.

(31) Wang, X.; Rodriguez, J. A.; Hanson, J. C.; Gamarra, D.; Fernandez-Garcia, M.; Martinez-Arias, A. *J. Phys. Chem. B* **2005**, *109*, 19595.

(32) Hammersley, A. P. *FIT2D: An Introduction and Overview*; ESRF Internal Report, ESRF97HA02T, 1997.

(33) Larson, A. C.; Von Dreele, R. B. *GSAS General Structure Analysis System*; Report LAUR 86-748; Los Alamos National Laboratory: Los Alamos, NM, 1995. (b) A. M. Reitveld, *J. Appl. Crystallogr*. **1969**, *2*, 65. (c) Toby, B. H. *J. Appl. Crystallogr.* **2001**, *34*, 210.

(34) (a) Newville, M.; Ravel, B.; Haskel, D.; Rehr, J. J.; Stern, E. A.; Yacoby, Y. *Physica B* **1995**, *208*−*209*, 154. (b) Ravel, B.; Newville, M. *J. Synchrotron Radiat.* **2005**, *12* (4), 537.

(35) Sayers, D. E.; Bunker, B. A. In *X-ray Absorption: Principles, Applications, Techniques of EXAFS, SEXAFS, and XANES*; Koningsberger, D. C., Prins, R., Eds.; John Wiley & Sons: New York, 1988; p 211.

(36) Kim, C. H.; Thompson, L. T. *J. Catal*. **2005**, *230*, 66.

(37) Fernández-García, M. *Catal. Rev.-Sci. Eng.* **2002**, *44*, 59.

(38) Henderson, M. A.; Perkins, C. L.; Engelhard, M. H.; Thevuthasan, S.; Peden, C. H. F. *Surf. Sci.* **2003**, *526*, 1.

(39) Padeste, C.; Cant, N. W.; Trimm, D. L. *Catal. Lett.* **1993**, *18*, 305.

(40) Otsuka, K.; Hatano, M.; Morikawa, A. *J. Catal.* **1983**, *79*, 493.

(41) Kundakovic, L.; Mullins, D. R.; Overbury, S. H. *Surf. Sci.* **2000**, *457*, 51.

(42) (a) Campbell, C. T.; Daube, K. *J. Catal.* **1987**, *104*, 109. (b) Nakamura, J.; Campbell, J. M.; Campbell, C. T. *J. Chem. Soc., Faraday Trans.* **1990**, *86*, 2725.

(43) Rodriguez, J. A.; Perez, M.; Evans, J.; Liu, G.; Hrbek, J. *J. Chem. Phys.* **2005**, *122*, 241101.

(44) Zhao, X.; Hrbek, J.; Rodriguez, J. A.; Perez, M. To be published.

(45) Martínez-Arias, A.; Hungría, A. B.; Fernández-García, M.; Conesa, J. C.; Munuera, G. *J. Power Sources* **2005**, *151*, 32.

(46) Li, C.; Sakata, Y.; Arai, T.; Domen, K.; Maruya, K.-i.; Onishi, T. *J. Chem. Soc., Faraday Trans 1* **1989**, *85*, 929.

(47) Li, C.; Sakata, Y.; Arai, T.; Domen, K.; Maruya, K.-i.; Onishi, T. *J. Chem. Soc., Faraday Trans 1* **1989**, *85*, 1451.

(48) (a) Bensalem, A.; Muller, J.-C.; Tessier, D.; Bozon-Verduraz, F. *J. Chem. Soc., Faraday Trans.* **1996**, *92*, 3233. (b) Dai, D.; Li, L.; Ren, J.; Whangbo, M.-H. *J. Chem. Phys.* **1998**, *108*, 3479.

(49) Meunier, F. C.; Tibiletti, D.; Goguet, A.; Reid, D.; Burch, R. *Appl. Catal.. A* **2005**, *289*, 104.